Inhibitors of PIM-1 Kinase: A Computational Analysis of the Binding Free Energies of a Range of Imidazo [1,2-b] Pyridazines

Slimane Doudou,[†] Raman Sharma,[†] Richard H. Henchman,[†,‡] David W. Sheppard,[†,§] and Neil A. Burton*[,†]

School of Chemistry, University of Manchester, Manchester, United Kingdom, M13 9PL, School of Chemistry, University of Manchester, Manchester, United Kingdom, M13 9PL, and BioFocus, Chesterford Research Park, Saffron Walden, United Kingdom, CB10 1XL

Received September 16, 2009

The binding of a selection of competitive imidazo [1,2-b] pyridazine inhibitors of PIM-1 kinase with nanomolar activity has been analyzed using computational methods. Molecular dynamics simulations using umbrella sampling to determine a potential of mean force have been used to accurately predict the relative free energies of binding of these inhibitors, from −4.3 to −9.5 kcal mol^{-1}, in excellent agreement with the trends observed in previous experimental assays. The relative activity of the inhibitors could not be accounted for by any single effect or interaction within the active site and could only be fully reproduced when the overall free energies were considered, including important contributions from interactions outside the hinge region and using explicit solvent in the active site. The potential of mean force for the displacement of the glycine-rich phosphate binding loop (P-loop) has also been estimated and shown to be an important feature in the binding of these ligands.

INTRODUCTION

Protein kinases are a major target for the development of small molecule inhibitors due to their particular importance for the treatment of cancer and inflammation. Among the many kinase targets actively being pursued,[1−5] there has been significant recent activity to target the PIM family of kinases.[4,6] The PIM gene has been identified as a proviral integration site for the Moloney murine leukemia virus and found to induce cell progression and to promote cell growth, with overexpression resulting in tumorigenesis.[7] This study focuses on the computational analysis of the binding of a specific range of inhibitors, imidazo [1,2-b] pyridazine ligands, originating from the BioFocus SFK33 library (see Figure 1) to one of the most important human kinases, PIM-1. This class of ligands has been previously shown to exhibit nanomolar potency for PIM-1 and for a 100-fold selectivity over PIM-2,[8] although the specific reasons for this activity are of current debate.

The PIM-1 kinase domain only binds its natural substrate adenosine triphosphate (ATP) through a single hydrogen bond due to the presence of a proline residue, Pro123, in the hinge region.[8,9] The presence of the proline residue differentiates PIM-1 from the majority of the kinome. Only five kinases share a proline in this position, and three of these are from the PIM family. The hinge region of the protein structure, illustrated in Figure 2 in red, is formed by residues Leu120, Glu121, Arg122, and Pro123 and is the usual target for ATP mimetic inhibitors,[10−13] particularly in other kinases where there is greater opportunity to exploit hydrogen-bonding interactions. Another important region of the PIM-1 structure is the presence of a glycine-rich phosphate binding loop (P-loop), shown in purple in Figure 2, which contains residues Gly45, Ser46, Gly47, Gly48, Phe49, and Gly50. This P-loop may be slightly displaced by the natural substrate, ATP, as suggested by the AMP−PNP inhibited structure.[14] In other kinases, the pliability of the P-loop has also been proposed to play an important role in the specificity and the affinity of inhibitors via an induced fit binding mode.[15,16] Unusually, the imidazo [1,2-b] pyridazines do not appear to bind in the same pose as ATP or other ATP mimetic inhibitors,[9,14,17] but bind at the opposite side of the ATP binding pocket, shown in blue in Figure 2, with relatively little displacement of the P-loop. The net result is a tertiary structure which strongly resembles that of the apoprotein, which may have important consequences for future inhibitor design, since the induced fit of inhibitors, such as AMP−PNP, may be energetically disfavored relative to inhibitors, which do not deform the structure significantly. This important aspect of binding will be addressed later when the energetic consequences for displacement of the P-loop will be considered.

Each imidazo [1,2-b] pyridazine ligand assessed in this paper has a common imidazopyridazine core with two substituents, R1 and R2 (see Figure 1). Two sets of ligands A and B, partitioned according to their R2 group, were selected for their diversity in ability to inhibit the enzyme; each set consists of six ligands, additionally labeled according to the R1 group. These ligands were selected to be representative of a larger ligand set whose relative solvation properties will also be assessed in this work, which have previously been screened by temperature shift assays.[18] This experimental approach is useful as a direct ligand binding assay for high-throughput inhibitor screening and takes

* Corresponding author. E-mail: neil.burton@manchester.ac.uk.
[†] School of Chemistry, University of Manchester.
[‡] Manchester Interdisciplinary Biocentre, University of Manchester.
[§] BioFocus.

10.1021/ci9003514
Published on Web 02/23/2010

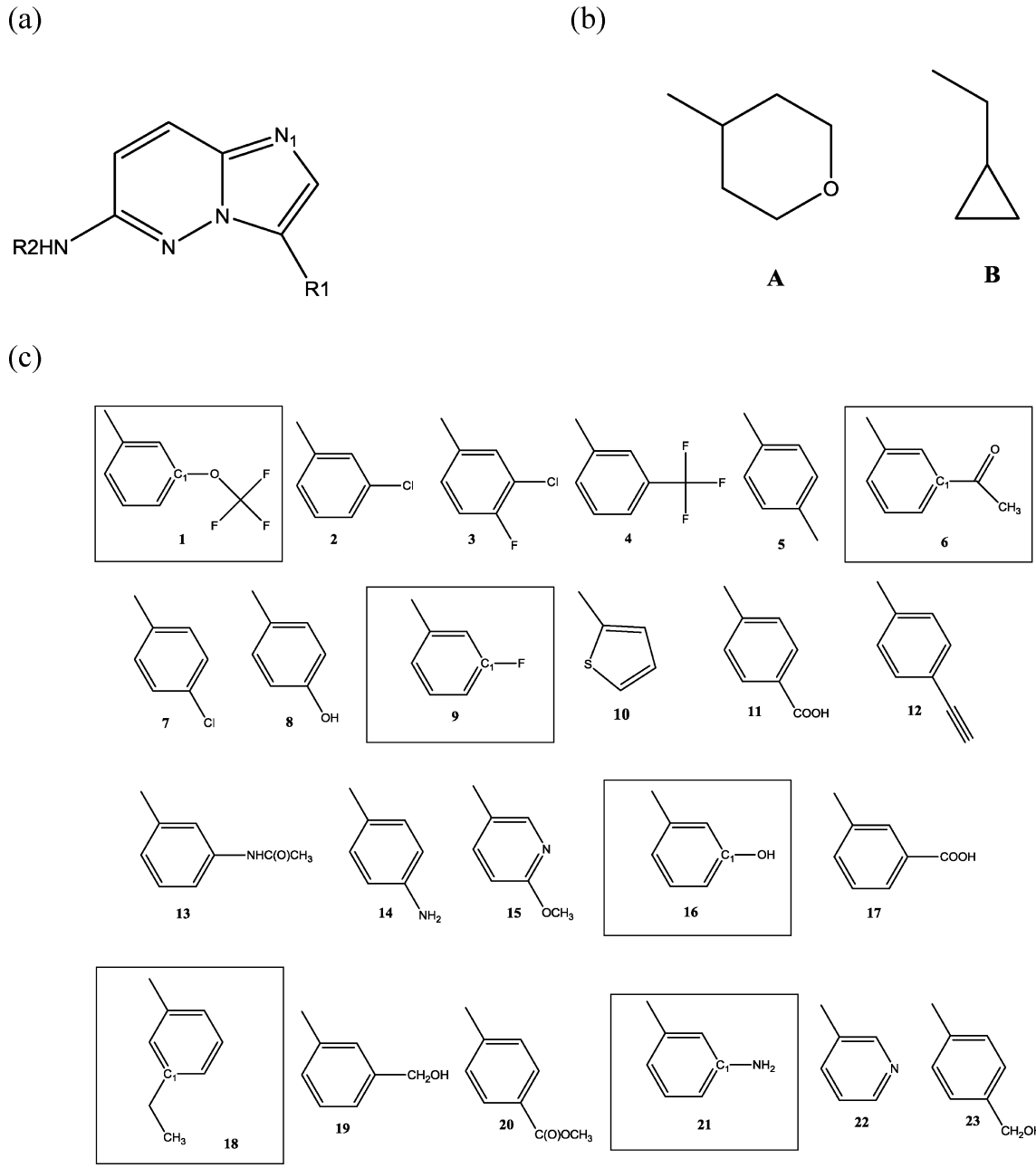

Figure 1. A range of imidazo [1,2-b] pyridazine inhibitors: (a) core; (b) the R2 groups; and (c) the general set of R1 groups (selected R1 groups used for detailed analysis are shown in boxes).

advantage of the assumption that binding ligands to proteins increases the protein thermal stability (or the melting temperature T_m) by an amount proportional to the concentration and affinity of the ligand.[8,19] In this approach, the reference temperature is taken to be the T_m of the unbound protein, and the ΔT_m data have been shown to correlate well with binding constants of PIM-1 from other experimental methods, such as isothermal titration calorimetry (ITC).[8]

A particular feature of this study will be the computation of the free energies of binding of a set of inhibitors where the differences in energy are anticipated to be difficult to discern by less intensive computational techniques. A wide variety of approaches have been used to model ligand inhibition of PIM kinases and to discuss their structure activity relationships.[20] These include the purely statistical evaluations from experimental data,[21] molecular modeling[10] or empirical scoring functions used in virtual high-throughput screening.[22] Each of these approaches has a role to play in the drug discovery process, but they often perform unreliably in terms of the accuracy of their prediction of binding free energies. In this study, we have chosen to use a relatively comprehensive free energy simulation approach,[23] since the differences between the activities of these ligands is known to be small, and the binding poses are proposed to be relatively similar. This approach will allow the direct determination of the potential of mean force (PMF) along a binding reaction coordinate connecting the bound structure to an unbound state.

The absolute binding free energy for ligand B6, imidazo [1,2-b] pyridazine 1 (also known by identifier K00135), has been previously determined experimentally using ITC,[8] which gives the binding free energy to be -9.8 kcal mol^{-1}. It was also noted that a moderate enthalpy of binding ΔH was observed and estimated to be -5.2 kcal mol^{-1}; this value

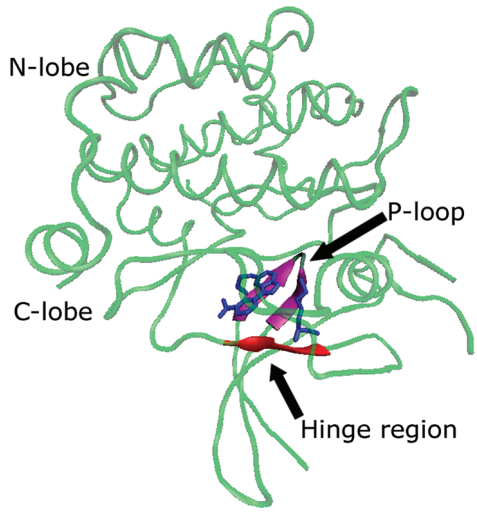

Figure 2. The PIM-1 kinase protein with the hinge region shown in red, the ligand B6 is shown in blue (on the left of Lys67 also in blue), and the P-loop is shown in purple.

was in contrast with other inhibitors of comparable activity such as BIM-1, a bisindolylmaleimide, where binding was found to be more strongly driven by enthalpy, with ΔG and ΔH being -10.4 and -14.3 kcal mol^{-1}, respectively. In the computational analysis presented here, we will show that the observed activities of these ligands rely upon a delicate balance of their desolvation and interaction energies, which must account for a number of important competing factors, including the position of the glycine-rich P-loop and the solvent within the active site. Although we have not explicitly analyzed the entropic contribution to the binding of these ligands in detail, the potential of mean force simulation approach employed indirectly accounts for the overall entropic contribution of ligand, protein, and solution.

The computational details of the three main modeling approaches utilized in this study are: (i) a quantum mechanical solvation model to assess the relative solubility of the full range of ligands; PMF simulations using a classical potential to determine; (ii) the binding free energies of selected ligands; and (iii) the free energy for displacement of the P-loop in the enzyme. We discuss the computed binding free energies of all 12 selected ligands and correlate these with the experimental binding data of Pogacic et al.[18] Our analysis clearly shows that both the absolute value and the differences in binding selectivity can be accurately predicted computationally and that the trends are predominantly explained by consideration of the nature of the R1 group, since the R2 substituents are similarly hydrophobic and have little effect on the selectivity. An important aspect, which we highlight in subsequent sections, is the analysis of the glycine-rich phosphate binding loop (P-loop) within the active site and the specific interactions of some ligands with it. A detailed breakdown of the binding energies to distinguish desolvation and enthalpic contributions are presented in order to explain the important distinguishing features of each bound ligand. These findings are of particular importance for the development of new ligand libraries for PIM-1 and other related kinase enzymes.

COMPUTATIONAL DETAILS

We have based our nomenclature for the ligands on that used in the experimental study[18] for ease of reference, retaining the ligand label of the R1 group, since this was based upon the numerical rank order of potency measured by the minimum observed value of the ΔT_m shift. We note that sets A and B used here correspond to R2 = 1 and R2 = 4, respectively, in reference;[18] for brevity the ligands are referred to by their R1 group code when the A or B set designation is not important to the discussion.

The starting coordinates used for all the PMF simulations were from the crystal structure of ligand B6 (K00135) bound to the PIM-1 kinase with PDB accession code 2C3I. There are no crystal structures for the other ligands bound to PIM-1, and the assumption that they have the same bound pose as ligand 6 was initially made, considering that all of the ligands are based on a similar core. The Gaussview program[24] was used to modify the R1 and R2 groups to generate the structure of each ligand in the binding site of PIM-1. The atomic charges of the ligands were produced using the AM1-BCC scheme of Antechamber in AMBER,[25−27] which is parametrized to reproduce HF/6-31G* RESP charges. Each system was set up using the AMBER03 force field[27] for the protein and solvated with the TIP3P water model with a buffer radius of 9 Å. Nine Na^+ ions were added to neutralize each system. The energy minimization and molecular dynamics (MD) simulations were performed with the Sander module of AMBER.[25] The periodic boundary conditions and the particle mesh Ewald method were used with a nonbonded cutoff of 9 Å. Each system was first energy minimized using 1000 steps of each of the steepest descent and conjugate gradient methods, subsequently followed by heating at a constant volume to 298 K in a 50 ps MD simulation and then equilibrated for 100 ps at a constant pressure of 1 bar. Bonds involving hydrogen atoms were constrained using the SHAKE algorithm, allowing a 2 fs integration time step.

To determine the binding free energy, we follow the general procedure discussed in detail previously.[23] We first compute the PMF along a binding reaction coordinate connecting the bound structure to an unbound state when the ligand is displaced by approximately 20 Å. At this distance, the unbound ligand is effectively fully solvated with very little interaction with the protein, so that a binding free energy can be obtained from the difference in the PMF of the bound and unbound (solvated) states. We stress that the final free energy of binding should be independent of the choice of this coordinate and, therefore, a linear (z-component) reaction path was chosen for ease of sampling, which minimized any ligand contacts with the binding site during the (un)binding event. The coordinate distance was taken to be the separation between the N_1 atom of the ligand (Figure 1) and the side chain nitrogen atom of Lys67, since this is a common hydrogen bond found in all ligand bound structures. Umbrella sampling was performed for 21 windows along the path starting at a N−N distance of 3 Å through to 23 Å. In each window, after displacing the ligand to the required N−N distance and after 1000 steps of minimization to remove any bad contacts, a 1 ns trajectory of restrained MD simulation was performed with force constants of 1 and 10 kcal mol^{-1} Å^{-2} for the z-component and the orthogonal

force constants, respectively. The PMFs were generated from the trajectories using the weighted histogram analysis method (WHAM)[19,20] and converted to standard free energies of binding using the method defined in refs 23, 28, and 29.

In order to assess the energetic penalties associated with displacement of the P-loop, a further PMF was computed in the absence of any ligand for a reaction coordinate defined as the distance between the α-carbons of Asp186 and Phe49 in the loop. Here the coordinate was partitioned into 14 windows (7.0−12.5 Å); each trajectory was equilibrated for 900 ps then sampled for 1.6 ns, with distances restrained using a harmonic umbrella potential and a force constant of 20 kcal mol Å^{-2}. The WHAM was used to generate the resulting PMF.

Although the umbrella-sampling simulations give us a direct prediction of the free energy of binding, it is useful to analyze the various factors which contribute to it. The following free energy cycle is often employed when computing binding free energies:

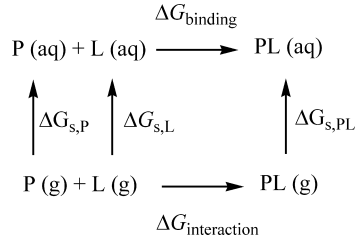

such that the observed standard free energy of binding ($\Delta G_{binding}$) can be approximated from the interaction energy between the protein (P) and the ligand (L) in the gas phase ($\Delta G_{interaction}$) and corrected by consideration of the solvation of the ligand ($\Delta G_{solvation}$):

$$\begin{aligned}\Delta G_{binding} &= G_{bound,aqueous} - G_{unbound,aqueous} \\ &= \Delta G_{interaction,gas\ phase} + \Delta G_{solvation}\end{aligned} \quad (1)$$

As eq 1 highlights, one of the major terms contributing to the binding efficacy is the solvation free energy difference, $\Delta G_{solvation} = \Delta G_{s,PL} - \Delta G_{s,P} - \Delta G_{s,L}$, which can be assessed independently of the interactions between the protein and ligand. Since we shall consider the relative binding energies of ligands which have relatively similar structures, entropic and protein solvation effects, which are accounted for in the PMF computations and are difficult to assess individually, are, thus, neglected in our analysis. To analyze how the observed inhibition efficacy of the ligands correlates with the various contributing interactions, we consider the energetic contributions using the following approximations and the usual assumption that $\Delta G_{s,PL} \approx \Delta G_{s,P}$:

$$\begin{aligned}\Delta G_{binding} &\approx \Delta H_{interaction,gas\ phase} + \Delta G_{solvation} \\ &\approx (H_{bound,gas\ phase} - H_{unbound,gas\ phase}) + \Delta G_{s,L}\end{aligned} \quad (2)$$

In order to initially assess how the solvation term may differentiate the ligands in general, we have computed the solvation energy of models corresponding to each of the 23 original R1 groups shown in Figure 1.[18] For each model of R1, a hydrogen atom was first added to satisfy valency, and then each was fully optimized using density functional theory with the B3LYP functional and the standard 6-31G* basis set, using the Gaussian quantum chemistry program.[30] Electrostatic solvation effects were included using the polarizable continuum model (PCM). In this approximation, a small ligand solvation energy, $\Delta G_{s,L}$, will be expected to favor inhibition, since the ligand is assumed to be fully desolvated when bound to the protein. The trends arising from this analysis will be discussed in the next section.

To assess the balance of solvation and interaction energy for each ligand in more detail, we have estimated $\Delta H_{interaction}$ using average force field potential energies of different snapshots taken from the window of the PMF MD simulations, where the ligand is bound

$$\Delta H_{interaction} \approx \langle E^{bound}_{W+P+L} \rangle - \langle E^{bound}_{W+P} \rangle - \langle E^{bound}_{L} \rangle \quad (3)$$

The first term is the potential energy of the whole solvated system, the second term is the potential energy of the protein (P) and the explicit solvent water molecules (W), and the last term accounts for the PE of the ligand (L) alone. For each ligand, we have taken the average of the energies of an ensemble of 200 snapshots (every 50 ps).

In addition to the analysis of the binding energy contributions, an estimate of the solvation interactions with each ligand, $\Delta H_{solvation}$, can be made in a similar way to that of the interaction energies using eq 4, taking the average energies from a window of the PMF MD simulations, where the structures are representative of the unbound state:

$$\Delta H_{solvation} \approx \langle E^{unbound}_{W+P+L} \rangle - \langle E^{unbound}_{W+P} \rangle - \langle E^{unbound}_{L} \rangle \quad (4)$$

The sum of $\Delta H_{interaction}$ and $\Delta H_{solvation}$ will approximate the binding enthalpy, ΔH_b, although this estimate will be more sensitive to the relative convergence in the sampling of the individual ΔH contributions. Although the solvation effects will be shown to be an important factor to understand the overall binding energies of these inhibitors, the various contributions to the interaction energies from specific amino acid residue−ligand interactions will ultimately be used to highlight the differences between the ligands. To assess these contributions, the potential energy for each protein−ligand interaction energy has been partitioned into individual residue−ligand contributions, which is possible due to the additive nature of the potential used, and was carried out using the ANAL module of the AMBER suite.

To assess the accuracy of the force field used, energies of the ligand bound to models of the active site were compared with semiempirical and density functional quantum mechanical values, which include empirical dispersion interactions. In each case, the empirical force field used for the PMF computations and the enthalpic analysis were shown to be accurate and reliable to within a few kcal mol^{-1}.[31]

Relative Solubility of the Ligands. A preliminary assessment of how the solvation contribution to binding influences the differential binding of the full set of ligands was carried out using a quantum mechanical approach; the solvation energy for all 23 R1 groups originally proposed by Pogacic et al. were estimated using the B3LYP/6-31G*/PCM method discussed in Section 2. In Figure 3, the experimental ΔT_m values are plotted against the predicted solvation free energy of each model R1 group. Note that in Figure 3, the negative of the solvation energy is plotted so that left to right correlates with an increase in the solvation

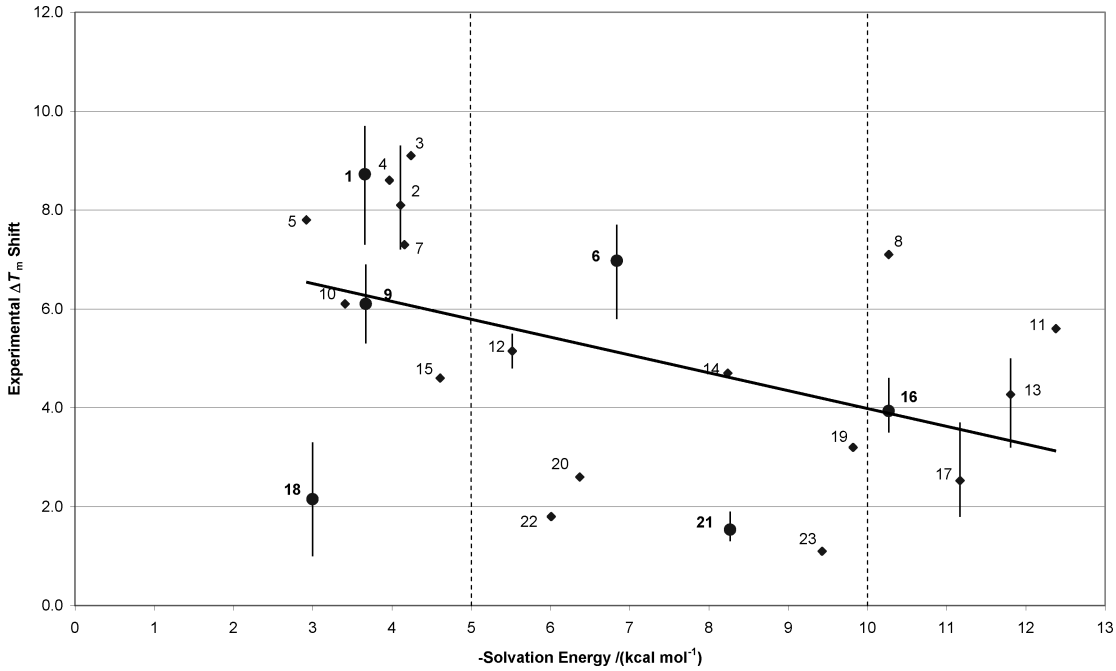

Figure 3. Solubility of the R1 side chain correlated with experimental ΔT_m shift data. The data points correspond to the average experimental ΔT_m shift value for R2 = 1,2,3, and 4, where data is available;[18] the bars correspond to the range of ΔT_m values. The circular data points indicate the ligands selected for further analysis.

of the ligand. Although there appears to be little correlation in the relationship between the inhibition and the solvation energy over the entire set of ligands, we have identified four groups of ligands, with those ligands selected for further study highlighted in bold:

- There is a cluster of ligands {**1**,2,3,4,5,7} where a large ΔT_m value naturally correlates with a low solvation energy.
- A wide range of ligands {**9**,10,12,13,14,15,**16**,17,19} which roughly follows the anticipated general trend that activity is decreased as the solvation energy increases.
- Ligands {**6**,8,11,**21**,23} are displaced from the second group although there are only single experimental ΔT_m values for 8,11 and 23.
- A group of ligands {**18**,20,22} where lower ΔT_m values do not particularly correlate with a high solvation energy.

In the PIM-1 kinase crystal structure (2C3I), there is evidence that one explicit solvating water molecule has been retained by the R1 carbonyl side chain of ligand B6 on binding to the protein. This suggests that the protein is able to accommodate water in the binding site and may mean that, for ligands where such an explicit water is a major contribution to the solvation energy in the unbound state, there will be a reduced desolvation penalty on binding with enhanced binding free energies.

In order to analyze these potential group correlations, two sets of ligands, A and B, were chosen to be representative of the breadth of the ligand binding and solvation energies and the experimental data available. Each set, consisting of the 6 ligands, highlighted in bold above, with R1 = 1, 6, 9, 16, 18, and 21 were subjected to a detailed analysis using molecular simulation and modeling methods, which will be discussed in the subsequent sections.

Free Energies of Binding. Potentials of mean force were computed for the six ligands in both set A {A1, A6, A9, A16, A18, A21} and set B {B1, B6, B9, B16, B18, B21} using the molecular dynamics protocols outlined in the earlier

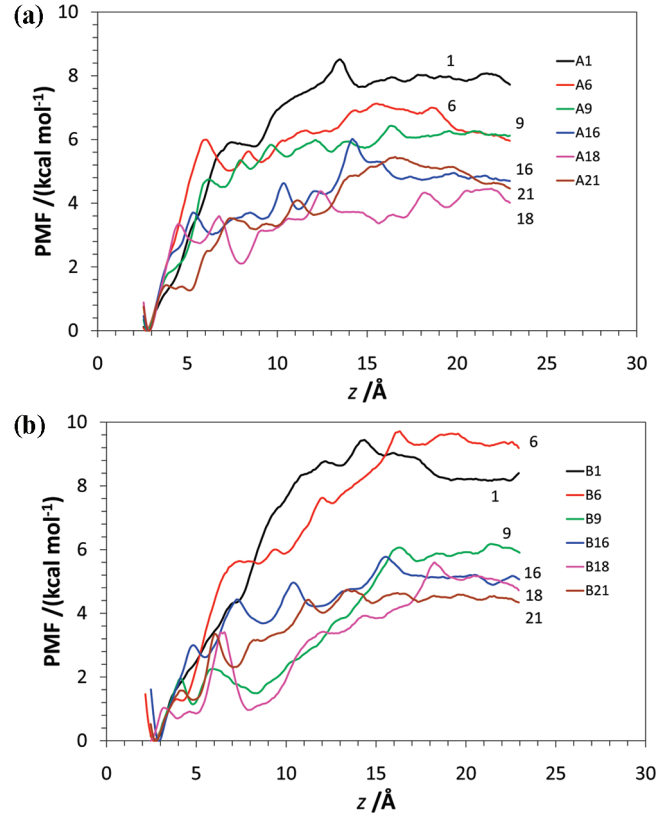

Figure 4. Potentials of mean force for: (a) ligand set A and (b) ligand set B.

sections. These will be referred to as PMF-A and PMF-B, which are shown in Figure 4a and b, respectively. ΔG_b has been determined from these PMFs as the difference between the PMF with the ligand bound minus the ligand when it is unbound. The binding energies have been summarized in Tables 1 and 2, respectively, for sets A and B and are relatively close in energy with values ranging from −4.5 to

Table 1. Binding Energies and their Contributions for Ligand Set A from PMF-A[a]

ligand	$\Delta H_{interaction}$	$\Delta H_{solvation}$	ΔH_b	ΔG_b	ΔT_m[b]
A1	−72.6 (±0.3)	−62.5 (±0.5)	−10.0 (±0.6)	−8.2	9.7
A6	−78.7 (±0.3)	−73.2 (±0.4)	−5.5 (±0.5)	−6.5	5.8
A9	−67.7 (±0.3)	−62.8 (±0.4)	−4.9 (±0.5)	−6.3	6.9
A16	−80.7 (±0.3)	−74.1 (±0.4)	−6.6 (±0.5)	−4.8	3.7
A18	−72.2 (±0.3)	−66.3 (±0.4)	−5.9 (±0.5)	−4.1	3.3
A21	−76.4 (±0.4)	−72.1 (±0.4)	−4.3 (±0.5)	−4.9	1.9

[a] The interaction ($\Delta H_{interaction}$) and solvation ($\Delta H_{solvation}$) energies, the enthalpy of binding (ΔH_b), and the binding free energies (ΔG_b) are in kcal mol^{-1}. The standard errors on the means are given in parentheses. [b] The experimental ΔT_m values were taken from ref 18.

Table 2. Binding Energies and their Contributions for Ligand Set B from PMF-B[a]

ligand	$\Delta H_{interaction}$	$\Delta H_{solvation}$	ΔH_b	ΔG_b	ΔT_m[b]
B1	−66.1 (±0.3)	−57.9 (±0.3)	−8.2 (±0.4)	−8.4	7.3
B6	−72.5 (±0.3)	−66.1 (±0.4)	−6.5 (±0.5)	−9.3	7.4
B9	−60.1 (±0.3)	−53.0 (±0.4)	−7.2 (±0.5)	−5.8	–
B16	−70.8 (±0.3)	−65.8 (±0.4)	−5.0 (±0.5)	−5.2	4.6
B18	−63.2 (±0.3)	−58.0 (±0.4)	−5.2 (±0.5)	−4.6	–
B21	−68.0 (±0.3)	−64.1 (±0.4)	−4.0 (±0.5)	−4.5	–

[a] The interaction ($\Delta H_{interaction}$) and solvation ($\Delta H_{solvation}$) energies, the enthalpy of binding (ΔH_b), and the binding free energies (ΔG_b) are in kcal mol^{-1}. The standard errors on the means are given in parentheses. [b] The experimental ΔT_m values were taken from ref 18.

−9.3 kcal mol^{-1}. Importantly, they closely follow the general trend shown in the experimental ΔT_m data: For set A, the ranking in order of binding efficacy is computationally (A1 > A9 ≈ A6 > A21 ≈ A16 > A18), and the ΔT_m data are (A1 > A9 > A6, A16 ≈ A18 > A21); for set B, the computational ranking is (B6 > B1 > B9 > B16 > B18 ≈ B21}, and the ΔT_m data are (B1 ≈ B6 > B16).

Our PMF energy difference, ΔG_b, for ligand B6 was computed to be −9.3 kcal mol^{-1}, which is very close to the experimental binding energy of Bullock et al., −9.8 kcal mol^{-1},[8] giving us confidence that the computational approach is accurately describing this binding event. If corrections to the PMF difference, to account for standard-state conditions, were to be included,[23] then $\Delta G^0_{binding}$ would be lower than ΔG_b by around 2 kcal mol^{-1} for this case; such discrepancies are undoubtedly compensated by the limitations of both the sampling and the force field employed. Since we would expect the corrections to be relatively similar for all of the ligands studied, uncorrected ΔG_b values will be used in subsequent discussions.

Before analyzing these data further, it is important to note that the ΔG_b values presented for ligands A1 and B1 were the result of resampled PMFs (PMF-A and PMF-B, respectively) based upon an alternative binding pose for the ligand. Although with exhaustive sampling a PMF should be independent of the starting conditions, the 1 ns sampling per window used here appeared to be insufficient to account for important conformational changes. For example, contrary to the experimental data, ΔG_b of ligand B1 was initially found to have considerably smaller magnitude than that of ligand B6, by around 5.0 kcal mol^{-1} when the PMF simulations were based upon a binding configuration similar to that of the crystal structure of B6, which we shall refer to as the B6-motif. To assess the possibility of important conformations which may not have been sampled during the constrained PMF trajectories and, in particular, the potential additional rotational freedom of ligand 1 and the response of the protein to it, an unconstrained MD simulation was performed for an additional 1 ns with ligand B1 bound in the protein. An average structure was constructed from this ensemble (using the PTRAJ module in the AMBER suite), and the main features of this new binding pose are shown in Figure 5. Visually there is relatively little difference between the new (redocked) pose and that of the original B6 pose, with the exception of the position of Phe49 in the P-loop. However, the energetic consequences of using the new structure as the initial configuration for the PMF are shown in Figure 6b, where there is significantly improved agreement of PMF-B with the experimentally predicted trend that B1 should have a comparable binding energy to B6. Indeed, the same effect was evident following a similar protocol for ligand A1, and the resulting binding energy for A1 is clearly larger than A6, in better agreement with the experimental trend. The new poses for ligand 1 will be considered in a later section where the importance of the P-loop is discussed in more detail. We should note that further resampling was not performed for the other ligands since they are of comparable size to ligand 6 without the rotational freedom of ligand 1, and analysis of the bound ensembles, particularly 9, 16, and 21, indicated that they are indeed likely to bind with a similar pose to B6.

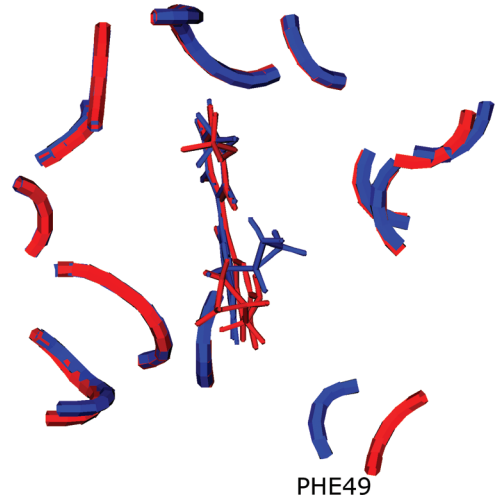

Figure 5. (a) Binding site configurations for ligand B1 in the assumed crystal structure motif (blue) and in the redocked configuration (red), and (b) the P-loop conformation for ligands B1 (redocked) and B6 (crystal structure).

To understand the interactions which govern the free energies of binding, we have estimated an enthalpic contribution based upon the ensembles of structures generated during the PMF simulations. Tables 1 and 2 summarize the various contributions following the computational approximations presented earlier. We note that ΔH_b for ligand B6, −6.5 kcal mol^{-1}, is in reasonable agreement with the experimental ITC value of −5.2 kcal mol^{-1} reported by Bullock et al,[8] and our value for ligand A6, −5.5 kcal mol^{-1}, is in good agreement with both of these values, as might be anticipated due to the similarity in their structures and binding poses. Comparing the estimated binding enthalpies across the ligand sets, there is some agreement with the rank order of ΔG_b for set B but less so with set A, which is perhaps

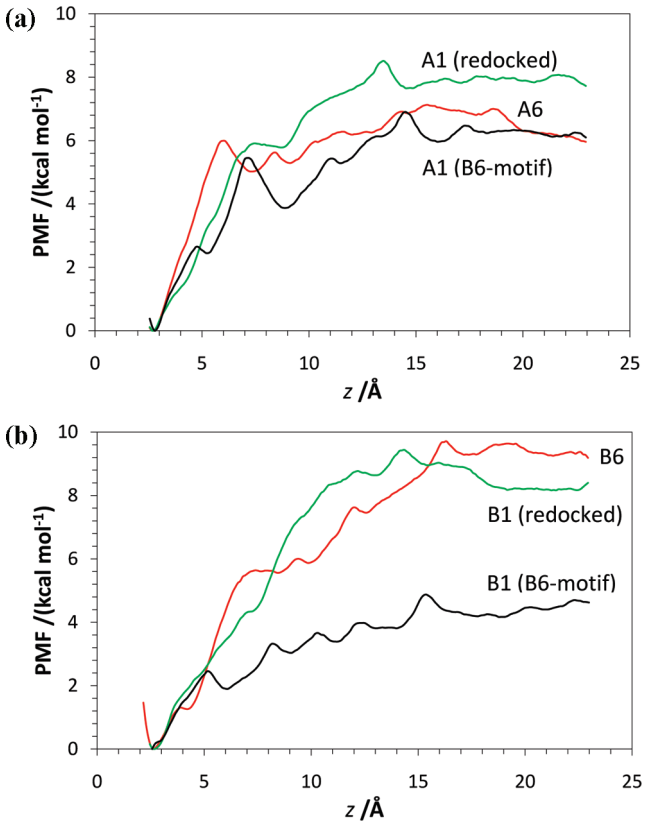

Figure 6. A comparison of the potentials of mean force for ligands (a) A1 and (b) B1, using simulations based upon an original B6-motif docked structure and a resampling from redocked-motifs.

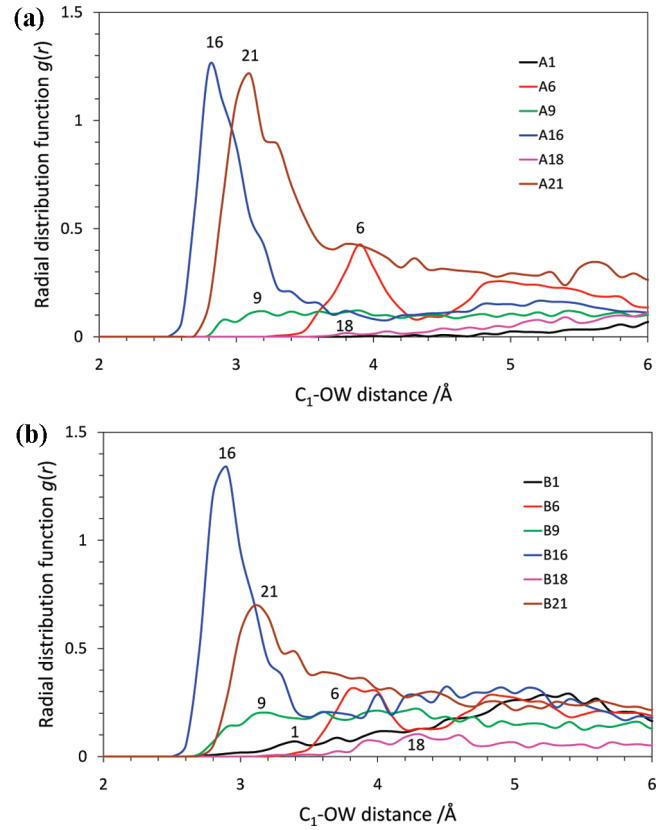

Figure 7. Radial distribution functions, for the oxygen atom of water molecules relative to the C_1 atom of the R1 group, in the PIM-1 binding pocket for: (a) ligands in the A set and (b) ligands in the B set.

unsurprising given the limited sample size and the small energy differences involved. Perhaps more illuminating are the two contributions to ΔH_b from binding and solvation, $\Delta H_{interaction}$ and $\Delta H_{solvation}$, respectively, which are shown in Tables 1 and 2. These relative energies are computed directly from either the bound or the unbound PMF simulation windows, respectively, and are less sensitive to the limited sampling, as shown by the standard errors.

First, considering $\Delta H_{solvation}$, we note that the rank order for sets A and B is very similar and closely follows the trend predicted by the free energies of solvation for the R1 groups discussed in the previous section, and so, we shall consider the ligands in terms of their R1 groups: ligands 1, 9, and 18 have the lowest solvation energies, and $6 \leq 21 \leq 16$, thus, confirming our hypothesis that the core and R2 groups do not significantly affect the relative desolvation of the ligands. It is clear from these data that ligand 1 is a better inhibitor than 18 purely on the basis of its more exothermic enthalpy of interaction. Ligand 9 appears to have the least exothermic $\Delta H_{interaction}$ of all of the set, but its binding energy cannot be explained by the bulk solvation differences, which suggests that it should have a very similar solvation energy to 1 and 18. For the other ligands, ligand 6 clearly has the most exothermic enthalpy of interaction, followed by ligand 16, and ligand 21 has the least exothermic, in line with their observed binding free energies. The specific interactions contributing to these energies will be discussed later.

Analysis of the Binding Interactions: Explicit Solvation and Enthalpies of Interaction. Desolvation on binding is clearly an important factor in differentiating the relative binding energies of these ligands, and it is interesting to analyze the interactions and energy, H_{LW}, which each bound ligand has with the water molecules in the binding site. These interactions were highlighted as potentially important features of the crystal structure of B6, where the binding site was seen to accommodate at least one explicit water molecule. Before considering the ligand−protein interactions in some detail, it is useful to explore the potential to retain explicit water−ligand binding in the binding site of the ligand set. Figure 7 shows the radial distribution function, g(R), where R was chosen as the C1-OW distance, where C1 is common to all ligand R1 side groups (see Figure 1), and OW is the oxygen atom of the water molecules in the binding sites. The peaks at approximately 3 Å for ligands 16 and 21 and at 4 Å for ligand 6 correspond to water molecules explicitly hydrogen bonded to the R1 group (O− or N− atoms) of the ligand. Ligands 1, 9, and 18 show no explicit solvation interactions, as might be expected.

Any explicit interactions with water in the binding site would generally be expected to reduce the desolvation penalty of ligands similar to B6 on ligand binding. H_{LW}, which averages the interactions between the ligand and water molecules within 5 Å of the ligand, is summarized in Table 3 for both ligand sets and has been estimated in this case from the PMF structures using an analogous approach to that used to partition $\Delta H_{interaction}$ into ligand−residue energies. From the H_{LW} values, we can discern that the more hydrophobic ligands, B1, B9, and B18, do exhibit lower energies than 6, 16, and 21, in agreement with the observed water radial distribution functions (see Figure 7). By taking the difference of H_{LW} and $\Delta H_{solvation}$, a desolvation penalty on binding can, thus, be approximated, which takes into

Table 3. Approximate Interaction Energies between the Protein and Ligand Set A[a]

ligand	H_{LW}	ΔH_{PL}	$\Delta H_{desolvation}$
1	−15.4 (−6.1)	−57.2 (−60.0)	47.2 (51.8)
6	**−19.9** (**−16.2**)	−58.8 (−56.3)	53.3 (49.9)
9	−14.7 (−12.3)	−53.0 (−47.8)	48.1 (40.7)
16	**−24.8** (**−22.0**)	−55.9 (−48.8)	49.3 (43.8)
18	−16.0 (−15.0)	−56.2 (−48.2)	50.3 (43.0)
21	**−27.6** (**−15.8**)	−48.8 (−52.2)	44.4 (48.2)

[a] Energies for set B are shown in parentheses. $\Delta H_{desolvation}$, H_{LW}, and ΔH_{PL} are the desolvation energies, ligand binding site water, and protein−ligand binding energies, respectively, in kcal mol^{-1}.

account that the complex can accommodate specific solvating interactions which would be present in bulk solution. The desolvation energies, $\Delta H_{desolvation}$, for other ligands are also presented in Table 3. Although there is some variation in the desolvation energies of sets A and B, there is no distinct trend which would suggest that desolvation is a main differentiating factor in the binding potency of these ligands. However, it is important to recognize that the more hydrophilic ligands in the set are all able to retain key ligand−water interactions on binding; for example, ligand 16 consistently gives a similar desolvation energy to its more hydrophobic counterpart, ligand 9, with values for set A of 48 and 49 kcal mol^{-1}, respectively. Set B has the same similarity.

In order to only take account of interactions between the protein and the ligand and to exclude the interactions between the ligand and the specific binding site water molecules, modified protein−ligand interaction energies, ΔH_{PL} are summarized in Table 3. Now it is ligands B1 and B6, the most potent ligands, that clearly have the greatest interactions with the protein and exhibit ΔH_{PL} values more exothermic than −56 kcal mol^{-1} for both sets. The remaining ligands appear to interact with the protein with similar energies ranging from −48 to −56 kcal mol^{-1} in set A and −48 to −50 kcal mol^{-1} in set B. In the next section, we shall look at the binding structures and the protein−ligand interactions in detail in order to explore the differences in the binding poses of these ligands.

Turning our attention to the specific binding interactions, which mediate the binding of these ligands with the protein binding site, we have analyzed the interaction energies of the ligand with the key residues in the binding site. Sixteen residues were selected (see Figure 8) which form the binding pocket for ligand B6 in the crystal structure. These residues have been partitioned into three sets of residues which closely interact with: (i) the core of the ligand; (ii) the R1 group; and (iii) the R2 group. The interaction energies, determined according to the method outlined in the computational details, are presented in Tables 4, 5, and 6, respectively, with significant contributions or notable trends shown in bold. Inspection of the interaction energies shows that there is clearly no single interaction which can be attributed to the difference between the ligands. It is clear that the hydrogen-bonding interaction of the ligand core (N) with Lys67, at −11 to −15 kcal mol^{-1}, is the most significant contribution, but there is no correlation with the overall binding enthalpy or free energy. The only other significant contributions are between the core and Ile185 at around −6.5 kcal mol^{-1} and the hydrophobic R2 group up to −8 kcal mol^{-1}, again with no distinguishing trends. Interestingly, there are no significant interactions with the hinge region (Leu120, Glu121, and Arg122) except for ligand 6, where the R1 group appears to strongly coordinate with Arg122, with a value in excess of −7 kcal mol^{-1} mainly through van der Waals and ligand carbonyl to C_β−H interactions. One interesting anomaly is the low interaction energy of the ligand 1 core with Phe49 in the P-loop; this value correlates with the observation that the P-loop is displaced to favorably accommodate ligand 1 in the binding site. The interaction of Phe49 with ligand B6 is a little greater at around −4 kcal mol^{-1} through increased T-shaped stacking with the core rings. The other interactions between the ligand and the binding site are generally less than 4 kcal mol^{-1}. Additional simulation of the binding pose of ligand B9 was performed to ensure a representative average interaction of this ligand with respect to Arg122 and Glu171, since a variety of conformations were energetically accessible within the hinge region due to the small R1 group, including an occasional unusual direct interaction with the side chain of Arg122. These small conformational differences were found to have no significant effect on the binding energetics. The subtle variety of the binding interactions of the ligands with these binding site residues can be seen in the Supporting Information (Figures S1, S2 and S3), which illustrate the averaged bound structures and the averaged distances of interest.

Semiempirical (PM3) quantum calculations, including empirical dispersion corrections, on a model of the active site containing each of the active-site side chains and the ligand B6 from the crystal structure confirm the most important interactions to be with Lys67, Arg122, and Glu171. Mutation of these residues to alanine gave differential interaction energies of −11, −9, and −6 kcal mol^{-1}, respectively, in good agreement with the interaction energies given by the empirical force field presented above.

Interactions with the Glycine-Rich P-Loop. An unusual aspect of the crystal structure (2C3I) of PIM-1 with ligand B6 (K00135) bound is that the glycine-rich P-loop appears to be in a similar conformation to that of the kinase tertiary apo-structure. To assess the importance of this loop position, it is useful to compare the various configurations of the loop based upon different crystallographic structures. Four 1 ns MD trajectories were performed starting from the crystal coordinates of: (a) 2C3I including the B6 ligand;[18] (b) 2C3I without B6; (c) 1YXT including the AMP−PNP (ATP mimetic) ligand;[14] and (d) 1YXT excluding AMP−PNP. These trajectories show that the P-loop position with no ligand bound can relax to a distance between the α-carbons of Asp186 and Phe49 of around 7−10 Å (see Figure 9) but is displaced to 12−14 Å upon inclusion of AMP−PNP. An almost identical trend is seen if we consider the alternative distance between the ring centroid of Phe49 and the C_α of Asp186, indicating that our observation is not affected by the orientation of Phe49.

Indeed the position of the P-loop is an interesting factor in the binding of the various ligands, and a similar analysis, averaging the C_α separation of Asp186 and Phe49, was performed on the trajectories taken from the windows with ligands bound and with ligands unbound, respectively, of the PMF-B simulations of the ligands in set B. These P-loop interaction distances are shown in Table 7 and indicate that each of the ligands B1, B6, B9, B16, B18, and B21 bind with minimum displacement of the P-loop, a separation of

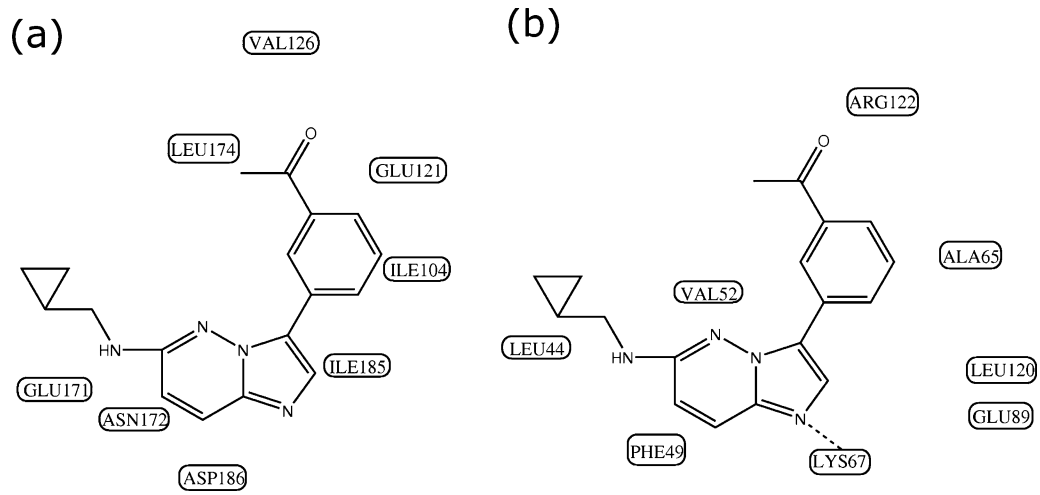

Figure 8. The location of key binding residues: (a) on the "left-hand side" of the binding site and (b) on the "right-hand side" of the binding site with ligand B6.

Table 4. Interactions between the Ligands in Set A and the Binding Site Residues Proximal to the Core of the Ligand[a]

ligand	Phe49	Val52	**Lys67**	Glu89	Leu120	**Ile185**	Asp186
1	**−1.4 (−1.5)**	−3.3 (−3.4)	**−12.6 (−13.7)**	3.6 (3.8)	−1.4 (−1.3)	**−6.7 (−7.0)**	**−4.3 (−3.4)**
6	−4.0 (−3.8)	−3.9 (−4.0)	**−12.3 (−12.6)**	3.0 (3.2)	−1.3 (−1.2)	**−6.4 (−6.1)**	−1.8 (−1.3)
9	−3.6 (−2.9)	−3.3 (−3.4)	**−13.9 (−14.5)**	3.8 (4.0)	−1.4 (−1.1)	**−6.6 (−6.1)**	−1.1 (−1.1)
16	−3.8 (−3.1)	−3.4 (−3.4)	**−14.2 (−15.4)**	4.3 (4.7)	−1.2 (−1.3)	**−6.6 (−6.0)**	−1.6 (−0.5)
18	−4.2 (−3.0)	−2.8 (−2.5)	**−15.1 (−16.7)**	4.5 (4.6)	−1.5 (−2.5)	**−5.6 (−7.2)**	−0.9 (0.4)
21	−3.5 (−1.6)	−3.2 (−3.2)	**−11.3 (−15.9)**	3.9 (5.2)	−1.2 (−1.3)	**−2.6 (−6.2)**	−2.4 (−1.0)

[a] Energies for set B are given in parentheses, and all energies are in kcal mol^{-1}. Interactions that exhibit significant interaction or notable trends are shown in bold font.

Table 5. Interactions between the Ligands in Set A and the Binding Site Residues Proximal to the R1 Group of the Ligand[a]

ligand	Ala65	Ile104	Glu121	Arg122	Val126	Leu174
1	−1.8 (−1.6)	−1.3 (−1.4)	−2.0 (−2.8)	−2.9 (−3.6)	−0.8 (−1.0)	−2.9 (−3.3)
6	−1.6 (−1.6)	−1.4 (−1.5)	−1.5 (−2.1)	**−7.6 (−7.0)**	−0.7 (−0.9)	−3.3 (−3.2)
9	−1.6 (−1.3)	−1.3 (−1.2)	−2.0 (−2.2)	−2.4 (−1.6)	−0.4 (−0.3)	−2.8 (−2.1)
16	−1.6 (−1.6)	−1.6 (−1.2)	0.3 (−1.3)	−5.2 (−1.3)	−0.4 (−0.4)	−2.7 (−2.2)
18	−0.9 (−0.4)	−1.2 (−2.7)	−0.6 (−0.5)	−0.7 (0.3)	−0.6 (−0.1)	−2.6 (−0.6)
21	−1.4 (−1.9)	−1.0 (−1.1)	−0.2 (−0.4)	−0.7 (−1.6)	−0.4 (−0.3)	−2.2 (−1.8)

[a] Energies for set B are given in parentheses, and all energies are in kcal mol^{-1}. Interactions that exhibit significant interaction or notable trends are shown in bold font.

Table 6. Interactions between the Ligands in Set A and the Binding Site Residues Proximal to the R2 Group of the Ligand[a]

ligand	Leu44	**Glu171**	Asn172
1	−0.2 (−0.2)	**−3.9 (−7.8)**	−0.9 (−0.6)
6	−0.1 (−0.2)	**−6.1 (−3.4)**	−0.7 (−0.8)
9	−0.2 (−0.2)	**−4.3 (−3.0)**	−0.7 (−0.8)
16	−0.2 (−0.3)	**−5.5 (−3.9)**	−0.8 (−0.9)
18	−0.3 (−0.2)	**−8.1 (−2.4)**	−1.4 (−0.7)
21	−0.4 (−0.4)	**−5.9 (−5.2)**	−0.9 (−1.0)

[a] Energies for set B are given in parentheses, and all energies are in kcal mol^{-1}. Interactions that exhibit significant interaction or notable trends are shown in bold font.

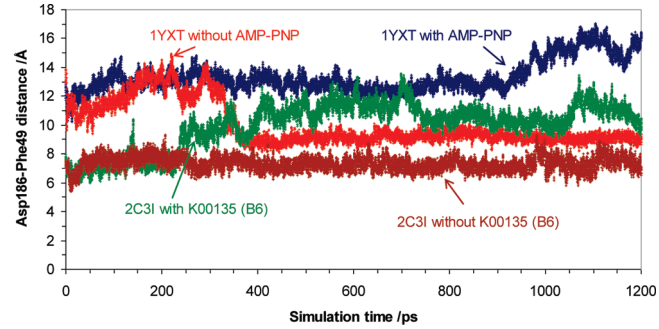

Figure 9. P-loop displacement during MD simulations of: (a) 2C3I including the B6 (K00135) ligand; (b) 2C3I without B6; (c) 1YXT including AMP−PNP; and (d) 1YXT excluding AMP−PNP. P-loop displacement is measured as the distance between the C_α atoms of Asp186 and Phe49.

less than 10 Å, and that there is relatively little induced strain due to binding, since the P-loop remains in the apo-like configuration when the ligand unbinds. The absolute values of the loop displacements given in Table 7, particularly for the unbound states, should be treated with some caution due to the limited sampling and the variance shown in the unrestrained simulations. For example, the unbound distance presented for ligand B1 is similar to that with the ligand bound, and we might expect the loop to relax to the shorter distances exhibited in the absence of the other ligands given sufficient time.

To assess the likely energy penalty required to displace the P-loop and to accommodate a ligand into the binding

Table 7. Displacement of the P-loop on Binding the B Ligand Set[a]

ligand	R_{bound}	$R_{unbound}$
B1	9.7	9.0
B6	7.0	7.7
B9	8.3	7.6
B16	8.4	6.4
B18	9.6	7.1
B21	9.8	6.8

[a] Average (C_α) separation (/Å) of Asp186 and Phe49 during the MD simulations with the ligand bound (R_{bound}) and unbound ($R_{unbound}$).

pocket, a PMF was computed for displacement of the loop in the apo-form of the protein. The details are outlined in Section 2, Computational Details, and the resulting PMF is shown in Figure 10 and shows a somewhat linear relationship between the free energy and the displacement distance. From the PMF, we can see that displacement of the P-loop can make a significant contribution to the overall binding energies of the ligands, and there is potentially a 13 kcal mol^{-1} free energy difference between the apo-like loop position, such as that with B6 (K00135) bound in 2C3I (7.3 Å), and the displaced loop (>12 Å) in the AMP−PNP bound 1YXT structure. It is, therefore, likely that ligands such as B6 and B9 are deriving some of their efficacy from their ability to bind without significant displacement of the loop (7.0 and 8.3 Å, respectively) and that ligands B18 and B21 may be somewhat disadvantaged, since the P-loop is slightly more displaced (>9 Å). Although ligand B1 clearly results in a displacement of Phe49, as discussed in the previous section, the enthalpic benefits of the different binding mode appear to outweigh the 4 kcal mol^{-1} penalty that we predict that this displacement would result in.

CONCLUSIONS

A simulation approach to determine potentials of mean force has been applied to predict the relative binding affinity of a range of similar imidazo [1,2-b] pyridazine inhibitors of PIM-1 kinase. Although computation of the PMF for a binding event is a relatively expensive approach for the study of protein−ligand interactions, it has been shown here to closely reproduce the experimentally observed binding trends between ligands which typically differ in their binding by a few kcal mol^{-1}. A detailed analysis of the simulation data has revealed a number of subtle factors which are responsible for the effective function of these inhibitors and which differentiate their relative activities. In particular, the competing contributions from solvation and protein−ligand enthalpic interactions have been assessed, and it is found that the protein−ligand interactions within the hinge region are only a minor factor in determining the efficacy of these ligands. Thus, the binding interactions which contribute to the relative affinities are principally those which are not associated with the hinge region for most of the ligands. We have shown that the trends observed in the temperature shift inhibition data can only be fully reproduced when overall binding free energies are considered, and these must take account of the penalties for desolvation involving water in the active site and displacement of the glycine-rich P-loop.

Although displacement of the P-loop away from the ATP binding site is not a highly energetic process, with fluctuations of the loop observed through natural thermal motion, ligands which can bind without significant displacement of the loop, such as the imidazo [1,2-b] pyridazine inhibitors, would experience a binding energy advantage in excess of 10 kcal mol^{-1} over inhibitors which require a degree of induced fit, such as the ATP natural substrate. In this case, the enthalpy of binding the imidazo [1,2-b] pyridazines studied here is not as optimal as for most existing ATP mimetic inhibitors but appears to be compensated by minimal displacement of the loop.

On the basis of solvation/desolvation effects alone, ligands 16, 21, and, to a lesser extent, 6 may have been expected to exhibit poorer inhibition than ligands 1, 9, and 18; however,

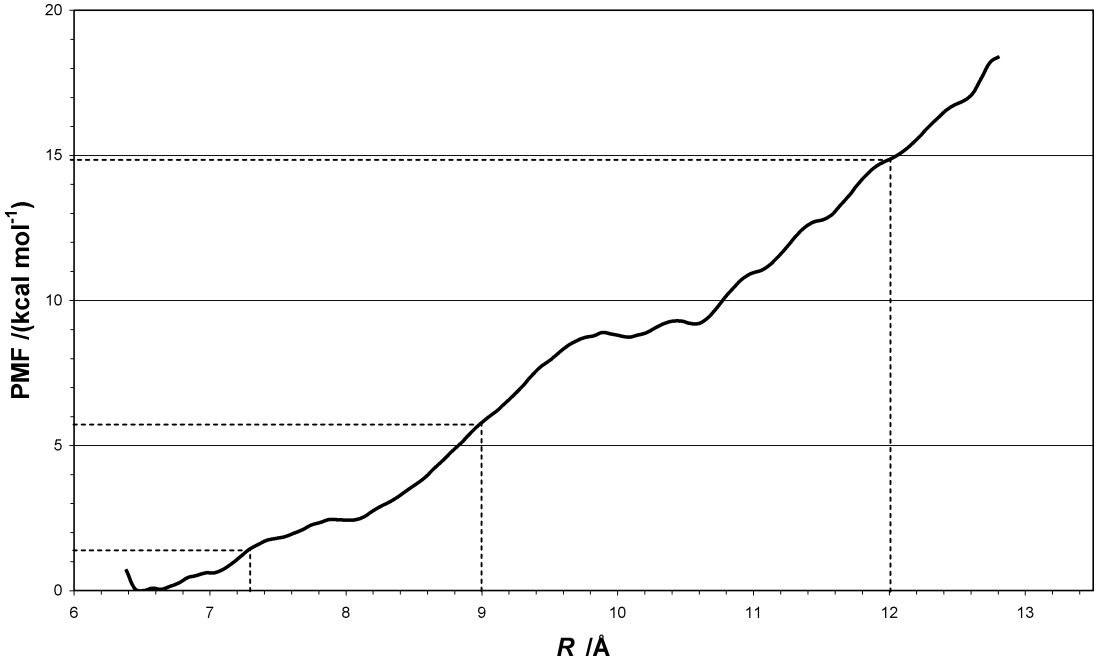

Figure 10. PMF for the displacement of the P-loop in 2C3I in the absence of ligand. R is the (C_α) separation (/Å) of Asp186 and Phe49.

they can maintain key solvent interactions when bound in the active site, thus, minimizing the desolvation necessary for them to enter what is generally a quite hydrophobic active site.

Analysis of the specific ligand interactions in detail has shown that ligands A6 and B6 (K00135), both containing the short keto side chain R1= 6, bind effectively due to a balance of factors; both have a low desolvation penalty on binding, since the binding site can accommodate specific solvent interactions with the carbonyl group while also exhibiting moderate enthalpic interactions within the binding site as well as a good interaction with Arg122 in the hinge region. It is also evident that the specific interactions of ligand 6 can be optimally made with little perturbation of the P-loop and that the resulting protein structure is, thus, similar to that expected of the apo-form. On the other hand, although ligand 1 can generally be considered to be the most effective inhibitor, this is mainly due to the relative hydrophobicity of its R1 group. Although this ligand has comparable or perhaps even slightly more favorable protein−ligand interactions with the binding site than the other ligands, it was found to be bound in a slightly different pose, thus, necessitating a small displacement of the P-loop. However, we have estimated that the free energy change to displace the loop, in this case, is relatively small and that the overall structure remains similar to that of the apo-form.

It is clear that the imidazo [1,2-b] pyridazine-based ligands are promising for the inhibition of PIM kinases since their binding pose, relative to ATP mimetic inhibitors, is quite unique by taking advantage of the kinase's P-loop. For the ligands assessed here it is clear that there are few large enthalpic interactions to dominate the binding, and there is clearly scope to optimize them to increase their activity.

ACKNOWLEDGMENT

We would like to thank Dr. John Harris and Professor Stefan Knapp for useful discussions. We are grateful for access to the NW Grid for computational resources and to the University of Manchester and EPSRC (DTA) for funding.

Supporting Information Available: Figures showing the average docked poses of the B-set of ligands. This material is available free of charge via the Internet at http://pubs.acs.org.

REFERENCES AND NOTES

(1) Zhang, J.; Yang, P.; Gray, N. Targeting cancer with small molecule kinase inhibitors. *Nat. Rev. Cancer* **2009**, *9* (1), 28–39.
(2) Bain, J.; Plater, L.; Elliott, M.; Shpiro, N.; Hastie, C.; McLauchlan, H.; Klevernic, I.; Simon, J.; Alessi, D.; Cohen, P. The selectivity of protein kinase inhibitors: a further update. *Biochem. J.* **2007**, *408* (3), 297–315.
(3) Fedorov, O.; Marsden, B.; Pogacic, V.; Rellos, P.; Mueller, S.; Bullock, A.; Schwaller, J.; Sundstroem, M.; Knapp, S. A systematic interaction map of validated kinase inhibitors with Ser/Thr kinases. *Proc. Natl. Acad. Sci. U.S.A.* **2007**, *104* (51), 20523–20528.
(4) Shah, N.; Pang, B.; Yeoh, K.-G.; Thorn, S.; Chen, C.; Lilly, M.; Salto-Tellez, M. Potential roles for the PIM1 kinase in human cancer - A molecular and therapeutic appraisal. *Eur. J. Cancer* **2008**, *44* (15), 2144–2151.
(5) Bamborough, P.; Drewry, D.; Harper, G.; Smith, G.; Schneider, K. Assessment of Chemical Coverage of Kinome Space and Its Implications for Kinase Drug Discovery. *J. Med. Chem.* **2008**, *51* (24), 7898–7914.
(6) Peng, C.; Knebel, A.; Morrice, N.; Li, X.; Barringer, K.; Li, J.; Jakes, S.; Werneburg, B.; Wang, L. Pim Kinase Substrate Identification and Specificity. *J. Biochem.* **2006**, *141* (3), 353–362.
(7) Morishita, D.; Katayama, R.; Sekimizu, K.; Tsuruo, T. Pim Kinases Promote Cell Cycle Progression by Phosphorylating and Down-regulating p27Kip1 at the Transcriptional and Posttranscriptional Levels. *Cancer Res.* **2008**, *68* (13), 5076–5085.
(8) Bullock, A. N.; Debreczeni, J. E.; Fedorov, O. Y.; Nelson, A.; Marsden, B. D.; Knapp, S. Structural Basis of Inhibitor Specificity of the Human Protooncogene Proviral Insertion Site in Moloney Murine Leukemia Virus (PIM-1) Kinase. *J. Med. Chem.* **2005**, *48* (24), 7604–7614.
(9) Qian, K.; Wang, L.; Cywin, C.; Farmer, B.; Hickey, E.; Homon, C.; Jakes, S.; Kashem, M.; Lee, G.; Leonard, S.; Li, J.; Magboo, R.; Wang, M.; Pack, E.; Peng, C.; Prokopowicz, A.; Welzel, M.; Wolak, J.; Morwick, T. Hit to Lead Account of the Discovery of a New Class of Inhibitors of Pim Kinases and Crystallographic Studies Revealing an Unusual Kinase Binding Mode. *J. Med. Chem.* **2009**, *52* (7), 1814–1827.
(10) Tong, Y.; Stewart, K.; Thomas, S.; Przytulinska, M.; Johnson, E.; Klinghofer, V.; Leverson, J.; McCall, O.; Soni, N.; Luo, Y.; Lin, N.-H.; Sowin, T.; Giranda, V.; Penning, T. Isoxazolo[3,4-b]quinoline-3,4(1H,9H)-diones as unique, potent and selective inhibitors for Pim-1 and Pim-2 kinases: Chemistry, biological activities, and molecular modeling. *Bioorg. Med. Chem. Lett.* **2008**, *18* (19), 5206–5208.
(11) Cheney, I. W.; Yan, S.; Appleby, T.; Walker, H.; Vo, T.; Yao, N.; Hamatake, R.; Hong, Z.; Wu, J. Z. Identification and structure-activity relationships of substituted pyridones as inhibitors of Pim-1 kinase. *Bioorg. Med. Chem. Lett.* **2007**, *17* (6), 1679–1683.
(12) Holder, S.; Zemskova, M.; Zhang, C.; Tabrizizad, M.; Bremer, R.; Neidigh, J. W.; Lilly, M. B. Characterization of a potent and selective small-molecule inhibitor of the PIM1 kinase. *Mol. Cancer Ther.* **2007**, *6* (1), 163–172.
(13) Xia, Z.; Knaak, C.; Ma, J.; Beharry, Z.; McInnes, C.; Wang, W.; Kraft, A.; Smith, C. Synthesis and Evaluation of Novel Inhibitors of Pim-1 and Pim-2 Protein Kinases. *J. Med. Chem.* **2009**, *52* (1), 74–86.
(14) Kumar, A.; Mandiyan, V.; Suzuki, Y.; Zhang, C.; Rice, J.; Tsai, J.; Artis, D. R.; Ibrahim, P.; Bremer, R. Crystal Structures of Proto-oncogene Kinase Pim1: A Target of Aberrant Somatic Hypermutations in Diffuse Large Cell Lymphoma. *J. Mol. Biol.* **2005**, *348* (1), 183–193.
(15) Yamaguchi, H.; Miwa, Y.; Kasa, M.; Kitano, K.; Amano, M.; Kaibuchi, K.; Hakoshima, T. Structural Basis for Induced-Fit Binding of Rho-Kinase to the Inhibitor Y-27632. *J. Biochem.* **2006**, *140* (3), 305–311.
(16) Gohda, K.; Hakoshima, T. A molecular mechanism of P-loop pliability of Rho-kinase investigated by molecular dynamic simulation. *J. Comput.-Aided Mol. Des.* **2008**, *22* (11), 789–797.
(17) Jacobs, M. D.; Black, J.; Futer, O.; Swenson, L.; Hare, B.; Fleming, M.; Saxena, K. Pim-1 Ligand-bound Structures Reveal the Mechanism of Serine/Threonine Kinase Inhibition by LY294002. *J. Biol. Chem.* **2005**, *280* (14), 13728–13734.
(18) Pogacic, V.; Bullock, A.; Fedorov, O.; Filippakopoulos, P.; Gasser, C.; Biondi, A.; Meyer-Monard, S.; Knapp, S.; Schwaller, J. Structural Analysis Identifies Imidazo[1,2-b]Pyridazines as PIM Kinase Inhibitors with In vitro Antileukemic Activity. *Cancer Res.* **2007**, *67* (14), 6916–6924.
(19) Matulis, D.; Kranz, J. K.; Salemme, F. R.; Todd, M. J. Thermodynamic Stability of Carbonic Anhydrase: Measurements of Binding Affinity and Stoichiometry Using ThermoFluor. *Biochemistry* **2005**, *44* (13), 5258–5266.
(20) Lamb, M. L.; David, C. S. Chapter 13 Targeting the Kinome with Computational Chemistry. In. *Annu. Rep. Comput. Chem.* **2005**, *1*, 185–202.
(21) Holder, S.; Lilly, M.; Brown, L. Comparative molecular field analysis of flavonoid inhibitors of the PIM-1 kinase. *Bioorg. Med. Chem.* **2007**, *15* (19), 6463–6473.
(22) Pierce, A.; Jacobs, M.; Stuver-Moody, C. Docking Study Yields Four Novel Inhibitors of the Protooncogene Pim-1 Kinase. *J. Med. Chem.* **2008**, *51* (6), 1972–1975.
(23) Doudou, S.; Burton, N. A.; Henchman, R. H. Standard Free Energy of Binding from a One-Dimensional Potential of Mean Force. *J. Chem. Theory Comput.* **2009**, *5* (4), 909–918.
(24) Dennington, R., II.; Keith, T.; Millam, J.; Eppinnett, K.; Hovell, W. L.; Gilliland, R. *GaussView, v3*; Semichem, Inc.: Shawnee Mission, KS, 2003.
(25) Case, D. A.; Darden, T. A.; Cheatham, T. E., III.; Simmerling, C. L.; Wang, J.; Duke, R. E.; Luo, R.; Merz, K. M.; Pearlman, D. A.; Crowley, M.; Walker, R. C.; Zhang, W.; Wang, B.; Hayik, S.; Roitberg, A.; Seabra, G.; Wong, K. F.; Paesani, F.; Wu, X.; Brozell, S.; Tsui, V.; Gohlke, H.; Yang, L.; Tan, C.; Mongan, J.; Hornak, V.; Cui, G.; Beroza, P.; Mathews, D. H.; Schafmeister, C.; Ross, W. S.; Kollman, P. A. *AMBER 9*, University of California: San Francisco, 2006.
(26) Jakalian, A.; Bush, B. L.; Jack, D. B.; Bayly, C. I. Fast, efficient generation of high-quality atomic charges. AM1-BCC model: I. Method. *J. Comput. Chem.* **2000**, *21* (2), 132–146.

(27) Duan, Y.; Wu, C.; Chowdhury, S.; Lee, M. C.; Xiong, G.; Zhang, W.; Yang, R.; Cieplak, P.; Luo, R.; Lee, T.; Caldwell, J.; Wang, J.; Kollman, P. A point-charge force field for molecular mechanics simulations of proteins based on condensed-phase quantum mechanical calculations. *J. Comput. Chem.* **2003**, *24* (16), 1999–2012.

(28) Kumar, S.; Rosenberg, J. M.; Bouzida, D.; Swendsen, R. H.; Kollman, P. A. The weighted histogram analysis method for free-energy calculations on biomolecules. I. The method. *J. Comput. Chem.* **1992**, *13* (8), 1011–1021.

(29) Dimelow, R. J.; Bryce, R. A.; Masters, A. J.; Hillier, I. H.; Burton, N. A. Exploring reaction pathways with transition path and umbrella sampling: Application to methyl maltoside. *J. Chem. Phys.* **2006**, *124* (11), 114113–114128.

(30) Frisch, M. J.; Trucks, G. W.; Schlegel, H. B.; Scuseria, G. E.; Robb, M. A.; Cheeseman, J. R.; Montgomery, J. A.; Vreven, T.; Kudin, K. N.; Burant, J. C.; Millam, J. M.; Iyengar, S. S.; Tomasi, J.; Barone, V.; Mennucci, B.; Cossi, M.; Scalmani, G.; Rega, N.; Petersson, G. A.; Nakatsuji, H.; Hada, M.; Ehara, M.; Toyota, K.; Fukuda, R.; Hasegawa, J.; Ishida, M.; Nakajima, T.; Honda, Y.; Kitao, O.; Nakai, H.; Klene, M.; Li, X.; Knox, J. E.; Hratchian, H. P.; Cross, J. B.; Adamo, C.; Jaramillo, J.; Gomperts, R.; Stratmann, R. E.; Yazyev, O.; Austin, A. J.; Cammi, R.; Pomelli, C.; Ochterski, J. W.; Ayala, P. Y.; Morokuma, K.; Voth, G. A.; Salvador, P.; Dannenberg, J. J.; Zakrzewski, V. G.; Dapprich, S.; Daniels, A. D.; Strain, M. C.; Farkas, O.; Malick, D. K.; Rabuck, A. D.; Raghavachari, K.; Foresman, J. B.; Ortiz, J. V.; Cui, Q.; Baboul, A. G.; Clifford, S.; Cioslowski, J.; Stefanov, B. B.; Liu, G.; Liashenko, A.; Piskorz, P.; Komaromi, I.; Martin, R. L.; Fox, D. J.; Keith, T.; Al-Laham, M. A.; Peng, C. Y.; Nanayakkara, A.; Challacombe, M.; Gill, P. M. W.; Johnson, B.; Chen, W.; Wong, M. W.; Gonzalez, C.; Pople, J. A. *Gaussian 03, D2*; Gaussian, Inc.: Pittsburgh, PA, 2003.

(31) Doudou, S. *Computational Modelling of Protein-Ligand Binding: Steps towards Better Drug Design*, Ph.D. Thesis, University of Manchester, Manchester, UK, 2009.

CI9003514